A missense mutation in podocin leads to early and severe renal disease in mice

A Philippe[1,2,9], S Weber[1,2,3,9], EL Esquivel[1,2], C Houbron[2,4,5,6], G Hamard[2,4,5,6], J Ratelade[1,2], W Kriz[7], F Schaefer[3], M-C Gubler[1,2] and C Antignac[1,2,8]

[1]Inserm, U574, Hôpital Necker-Enfants Malades, Paris, France; [2]Université Paris Descartes, Faculté de Médecine René Descartes, Paris, France; [3]Division of Pediatric Nephrology, Hospital for Pediatric and Adolescent Medicine, Ruperto-Carola University, Heidelberg, Germany; [4]Homologous Recombination Laboratory, Institut Cochin, Paris, France; [5]Inserm, U567, Paris, France; [6]CNRS, UMR 8104, Paris, France; [7]Institute for Anatomy and Cell Biology, Ruperto-Carola University, Heidelberg, Germany and [8]Department of Genetics, Hôpital Necker-Enfants Malades AP-HP, Paris, France

Mutations in the *NPHS2* gene, encoding podocin, are responsible for familial autosomal recessive and sporadic cases of steroid-resistant nephrotic syndrome. We have successfully generated a mouse model in which the common p.R138Q mutation found in nephrotic patients is expressed in the kidney. Homozygous mice express the mutant protein, which is mislocated to the cytoplasm, along with a portion of the nephrin pool. These mice die within the first month of life, but their survival depends on the genetic background. Albuminuria manifests early and leads to progressive renal insufficiency, characterized histologically by diffuse mesangiolysis and mesangial sclerosis, endothelial lesions along with podocyte abnormalities such as widespread foot process effacement. Gene expression profiling revealed marked differences between these and the podocin-null mice, including significant perturbations of podocyte-expressed genes such as *Cd2ap*, *Vegfa* and the transcription factors *Lmx1b* and *Zhx2*. Upregulation of *Serpine1* and *Tgfb1* implicates these as potential mediators of disease progression in these mice. This mouse model of nephrotic syndrome may serve as a valuable tool in studies of *in vivo* intracellular protein trafficking of podocyte proteins, as well as testing therapeutic modalities aimed at correcting the targeting of mutant proteins.

Kidney International (2008) **73,** 1038–1047; doi:10.1038/ki.2008.27; published online 20 February 2008

KEYWORDS: nephrotic syndrome; podocyte; genetic renal disease

Correspondence: *C Antignac, Inserm, U574, Hôpital Necker-Enfants Malades, 6ème étage, Tour Lavoisier, 147, rue de Sèvres, Paris 75015, France. E-mail: antignac@necker.fr*

[9]In our opinion, these individuals should be considered co-first authors of this manuscript

Received 12 October 2007; revised 27 November 2007; accepted 4 December 2007; published online 20 February 2008

Efforts over the past decade aimed at unravelling the genetic basis of nephrotic syndrome have led to significant advances in our understanding of the molecular basis of glomerular function and the pathophysiological mechanisms leading to proteinuric renal diseases. The *NPHS2* gene, encoding the slit diaphragm protein podocin, has been shown to be mutated in familial forms of autosomal recessive steroid-resistant nephrotic syndrome (SRNS),[1] and in sporadic cases.[2,3] Although early[4] and adult-onset[5] forms have been described, SRNS most commonly manifests between 3 and 6 years of age,[1] rapidly progresses to end-stage renal disease, and does not recur after transplantation. Mutations may involve both N- and C-terminal intracytoplasmic regions of the protein, and include both loss-of-function mutations as well as missense changes.[2] Indeed, the most commonly found variant is the p.R138Q mutation, observed in 32% of all affected alleles,[2] and leads to a severe, early-onset form.[4] Missense variants of podocin have been studied in cell culture models and some, including the p.R138Q mutation, have been shown to result in intracellular trafficking defects of podocin, whereas some are able to maintain plasma membrane targeting.[6] Moreover, podocin has been shown to function not only as a scaffold necessary for slit diaphragm assembly via its interactions with CD2AP and nephrin,[7] but also in nephrin targeting to lipid rafts, where signal transduction events occur.[8] Missense podocin variants have been shown to differ in their ability to affect nephrin trafficking to lipid rafts and plasma membrane.[9,10] More recently, podocin has been shown to bind to cholesterol regulating the activity of the transient receptor potential channel 6.[11]

Murine models have proven to be invaluable tools in elucidating the pathophysiological mechanisms leading to renal disease. Indeed, we have previously inactivated the murine *Nphs2* gene and showed that these mice develop early, and severe terminal renal disease, which differs phenotypically from disease seen in humans.[12] We have, therefore, developed a mouse model expressing the murine equivalent of the missense variant p.R138Q to better understand the

pathophysiological mechanisms involved in renal disease caused by mutant forms of podocin. These mice developed renal disease similar to that of the *Nphs2*-null model, due to failure of the mutant protein to target properly in the podocyte. We further demonstrated that survival can be modulated by genetic background and that the renal disease results in significant perturbations of gene expression in the kidney.

RESULTS

Successful targeting leads to expression of the R140Q podocin variant

The *Nphs2* gene in mice encodes a protein with 385 amino acids, two amino acids more than the human homolog. To generate a mouse model bearing a mutant R140Q variant of the podocin gene, corresponding to the p.R138Q mutation found in humans, a 6.6-kb targeting construct was generated, in which the c.505G > A, c.506A > G mutations were achieved by site-directed mutagenesis of exon 3 of the *Nphs2* gene, and a floxed *phosphoglycerate kinase–hygromycin* cassette was inserted into intron 3 for positive selection (Figure 1a). Successful homologous recombination in 2/299 embryonic stem cells was verified by Southern blot hybridization (Figure S1) and two embryonic stem cell clones were expanded and subsequently injected into C57BL/6 blastocysts. Germline transmission of the mutant allele was achieved by mating of >80% chimeric mice from one clone and verified by polymerase chain reaction (PCR) genotyping. Heterozygous $Nphs2^{R140Q/+}$ mice were crossed with Meu-Cre40 mice constitutively expressing Cre recombinase,[13] leading to excision of the floxed hygromycin cassette. Finally, the *Cre* allele was selected against by breeding heterozygotes with wild-type mice.

In the mixed C57BL/6:129SvPas background, inheritance of the mutant allele deviated from expected Mendelian ratios, with 65/351 (18.5%) $Nphs2^{R140Q/R140Q}$ genotyped at birth ($\chi^2 = 8.11$, 2 df, $P = 0.0173$), suggesting intrauterine or perinatal mortality. Expression of the mutant *Nphs2* transcript in $Nphs2^{R140Q/+}$ and $Nphs2^{R140Q/R140Q}$ mice was verified by sequencing the PCR products obtained after reverse transcription of total RNA extracted from kidneys (Figure 1b). By northern blot hybridization, no alternative splice variants were seen in mutant *Nphs2* mice, but *Nphs2* transcriptional levels were higher than in wild-type mice (Figure 1c). Real-time PCR confirmed significant upregulation of the *Nphs2* transcript at postnatal (P) day 4 and at P12, although the latter did not achieve statistical significance (Figure 1d). These results confirmed successful targeting of the *Nphs2* gene leading to expression of a podocin variant at biologically relevant levels.

Mutant R140Q podocin is mislocalized, along with nephrin

Despite higher levels of *Nphs2* mRNA in targeted mice, western blotting revealed an overall decrease in the expression of podocin at the protein level as early as P1 (data not shown), which was sustained at P12 (Figure 2). Previous studies have revealed that the p.R138Q human podocin variant, when overexpressed in cell culture models, fails to localize to the plasma membrane and is retained in the endoplasmic reticulum.[6,10] We, therefore, investigated the localization of podocin in homozygous $Nphs2^{R140Q/140Q}$ mice by immunofluorescence. In wild-type mice, anti-podocin antibodies labelled podocytes in a pattern consistent with plasma membrane expression, in close juxtaposition to the glomerular basement membrane marked by nidogen (Figure 3a). In $Nphs2^{R140Q/R140Q}$ mice, however, podocin no longer colocalized with nidogen, instead displayed an intracellular pattern of expression with perinuclear staining, indicating retention in the endoplasmic reticulum (Figure 3a). Additionally, in mutant mice, partial colocalization of nephrin with mutant R140Q podocin suggests that the intracellular trafficking defect of podocin leads to mislocalization of a fraction of the nephrin in podocytes (Figure 3b).

Mutant mice develop proteinuria and early, terminal renal failure

Thereafter, cohorts of mutant R140Q mice were followed till death or were killed at the designated time points. Heterozygous $Nphs2^{R140Q/+}$ mice followed to 1 year of age did not demonstrate albuminuria and had no obvious renal histological abnormalities (data not shown). Homozygous mutant mice on the mixed genetic background died at a median age of 4 days (range 1–40 days), with additional mice likely dying either *in utero* or in the perinatal period (Figure 4a). Previously, we had demonstrated a modifying effect of genetic background on the survival of *Nphs2*-null mice.[12] We, therefore, backcrossed the mutant $Nphs2^{R140Q}$ allele, enriching for 129S2/SvPas alleles, and the mice died at a median age of 14 days, significantly later than mixed background mice (Figure 4a). Furthermore, we identified 37/133 (27.8%) newborn $Nphs2^{R140Q/R140Q}$ mice on the 129-enriched background, which suggests insignificant perinatal mortality and is consistent with Mendelian inheritance.

Although appearing normal at birth, $Nphs2^{R140Q/R140Q}$ newborn mice quickly developed albuminuria, which progressed with age (Figure 4b). Biochemical measures of renal function in 129 mutant mice demonstrated significant elevations in plasma urea at both P4 and P12 (Figure 4c). Similarly, plasma creatinine was elevated at P4 but not P12 (Figure 4d). This may potentially be accounted for by a trend toward decrease in body weight at P12 in mutant podocin (9.67 ± 0.78 mg in controls vs 6.92 ± 0.96 mg in mutants, $P = 0.06$), which may reflect loss of muscle mass. These data are consistent with early and significant impairment of renal function in $Nphs2^{R140Q/R140Q}$ mice, and a potential role for genetic modifiers in determining the length of survival.

Evolution of renal histological lesions in mutant mice

Thereafter, we characterized the evolution of renal histological lesions in mutant mice and compared these with littermate controls (Figures 5a and b). Despite the early onset of albuminuria, light microscopy revealed no glomerular or

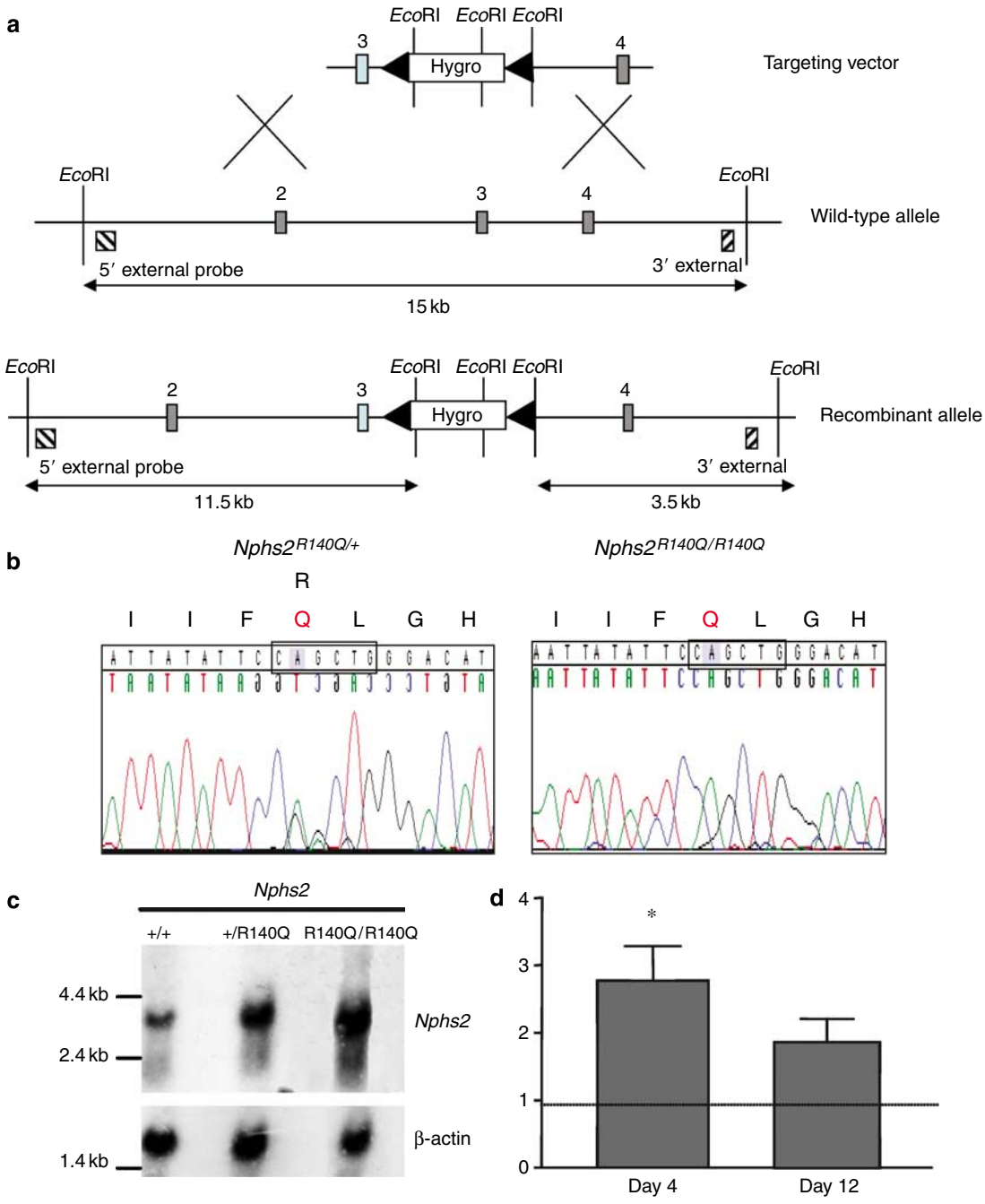

Figure 1 | Successful targeting of the murine *Nphs2* allele resulting in expression of a mutant R140Q podocin. (**a**) Schematic representations of the 6.6-kb targeting vector containing a modified exon 3 (light blue box) and a floxed phosphoglycerate kinase-hygromycin cassette, the genomic structure of wild-type murine *Nphs2* allele, and the allele resulting from homologous recombination. Exons are represented by closed gray boxes. *Eco*RI restriction sites, the locations of internal and external probes, and the resulting digestion products are noted. (**b**) Sequencing of PCR products, containing exon 3 of *Nphs2*, from $Nphs2^{R140Q/+}$ and $Nphs2^{R140Q/R140Q}$ kidneys demonstrating the mutant allele in the heterozygous and homozygous states. The *Pvu*II restriction site is indicated by a black rectangle. The amino acid reading frame is indicated above the chromatogram. (**c**) Northern blot of total RNA from kidneys of $Nphs2^{+/+}$, $Nphs2^{R140Q/+}$, and $Nphs2^{R140Q/R140Q}$ mice at P1 demonstrating increased expression of the 3.1-kb *Nphs2* transcript in mutant mice. A 1.8-kb β-actin transcript was used as a loading control. (**d**) Real-time PCR of *Nphs2* confirmed an increase in *Nphs2* mRNA levels in mutant mice ($n=6$ at P4, $n=5$ at P12) compared with controls ($n=5$ at each time point). * Denotes $P<0.05$ by *t*-test.

tubular abnormalities during the first three days of life (data not shown). At P4, surface hemorrhages were present in the kidneys of $Nphs2^{R140Q/R140Q}$ mice corresponding to focal areas of interstitial hemorrhages in the superficial cortex and juxtamedullary areas (Figure 5c). Mesangial expansion and focal areas of mesangiolysis were observed (Figure 5d), along with focal dilatations of capillary lumina, but podocytes appeared normal. Protein droplets were observed in proximal

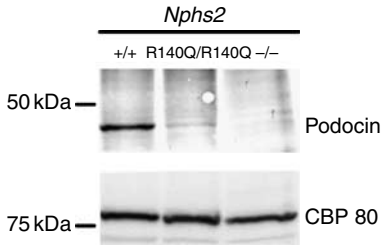

Figure 2 | Podocin levels are decreased in mutant mice. Western blotting using protein lysates from wild-type and *Nphs2*$^{R140Q/R140Q}$ mice at P12 showing a decrease in podocin expression in kidneys. Proteins from the kidney of an *Nphs2*$^{-/-}$ mouse were used as a negative control and CBP80 as loading control.

tubules along with focal tubular dilatation (Figure 5e). Arteries and arterioles were normal.

Mesangiolysis further worsened by P12, along with the presence of mesangial sclerosis, reducing the patency of capillary lumina (Figure 5f). Retraction of some sclerotic glomeruli was observed, without adhesions to Bowman's capsule. Glomerular lesions were associated with tubular alterations involving primarily the proximal tubules. These tubules showed varying degrees of dilatation and the presence of protein casts (Figure 5g). Mice killed at later time points (up to 32 days) showed globally sclerotic and obsolescent glomeruli, with severe and extensive tubulointerstitial lesions (Figure 5h).

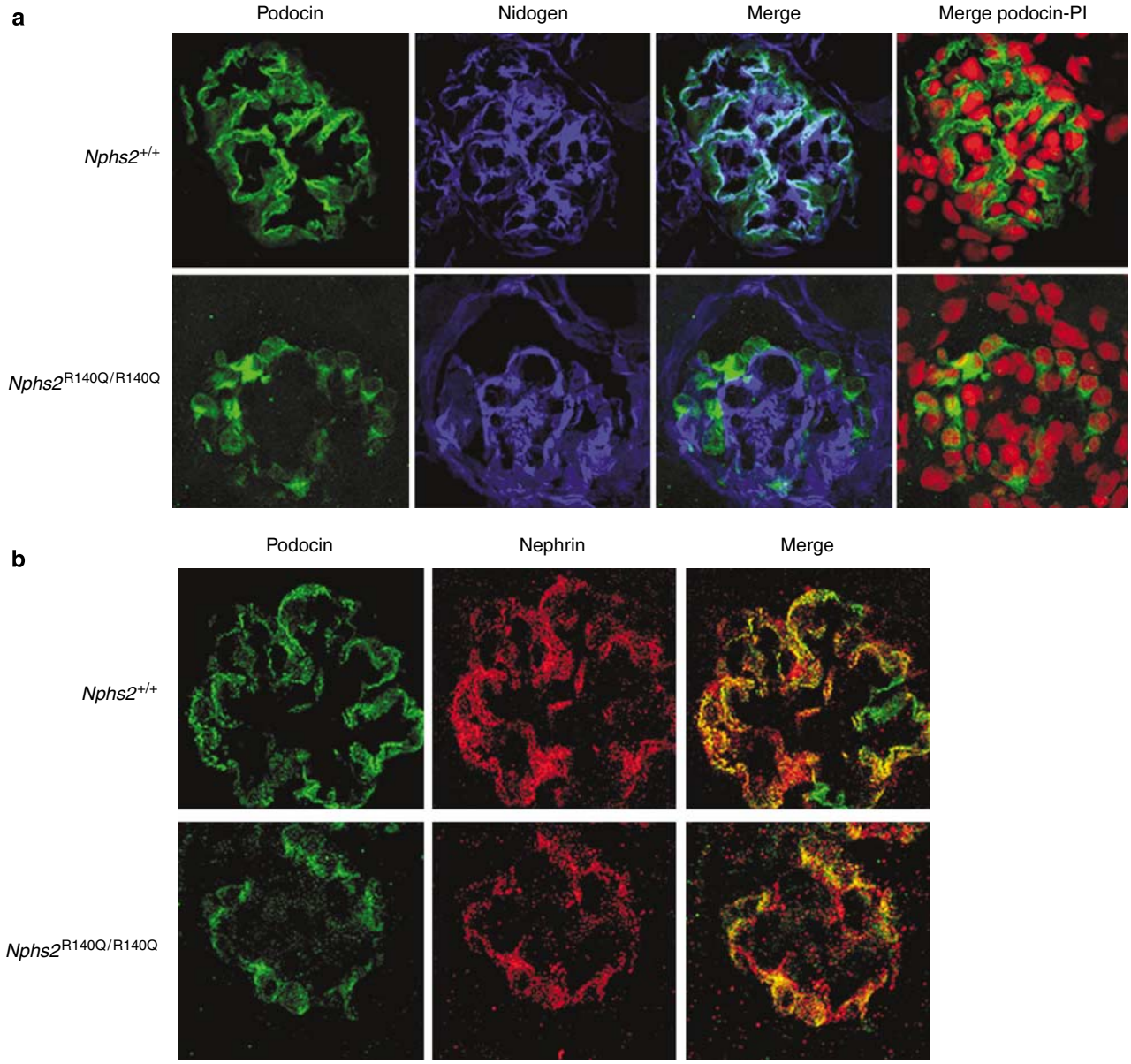

Figure 3 | Mutant R140Q podocin is mislocalized in the kidney, along with nephrin. (**a**) Confocal images showing podocin (in green) plasma membrane staining in wild-type mice in close apposition to the glomerular basement membrane labelled with nidogen (in blue). In contrast, mislocalization of podocin occurs in mutant mice at P4, with a perinuclear staining pattern (in relation to propidium iodide-stained nuclei in red), suggesting retention of mutant podocin in the endoplasmic reticulum. Original magnification ×630. (**b**) Double immunolabelling with podocin (in green) and nephrin (in red) demonstrates partial colocalization in both wild-type and mutant mice at P4 suggesting nephrin pool mistargeting. Original magnification ×630.

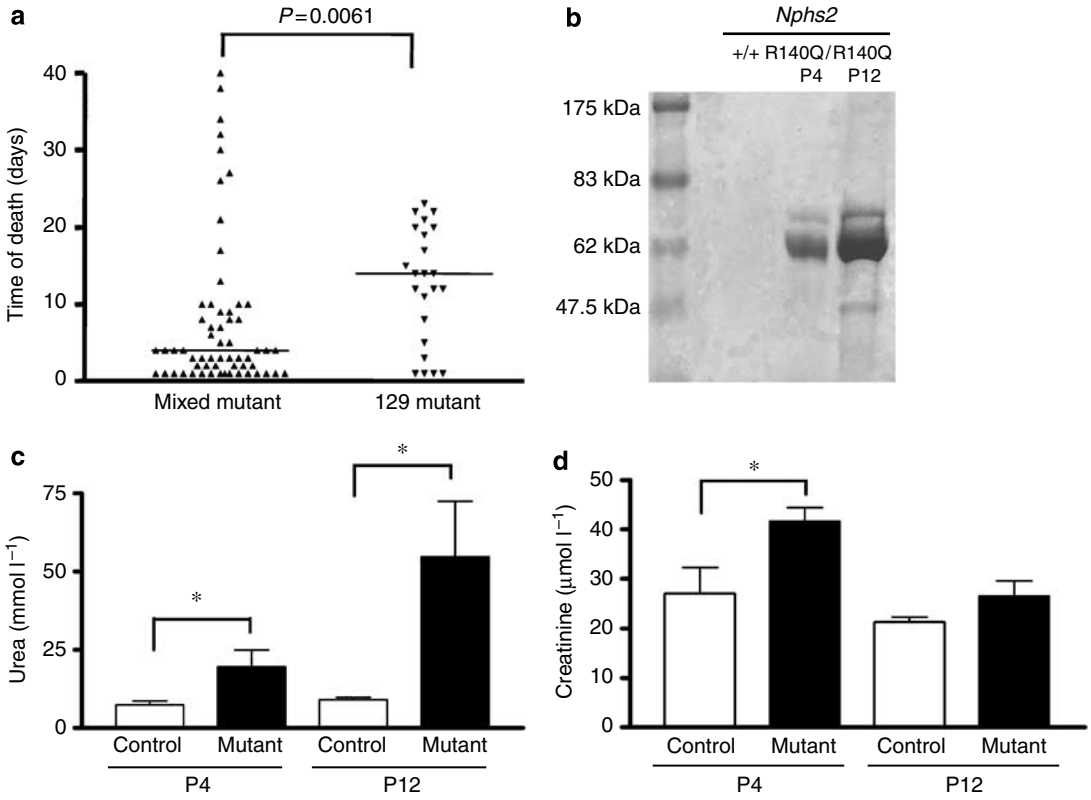

Figure 4 | Early mortality and renal insufficiency develop in mutant podocin mice. (**a**) Mortality in *Nphs2*$^{R140Q/R140Q}$ mice in the mixed and 129-enriched genetic backgrounds. (**b**) Coomassie blue-stained gel of urines from wild-type and mutant mice showing presence of albuminuria at P4, progressing to non-selective proteinuria by P12. (**c**) Early and sustained elevation in plasma urea in mutant mice at P4 and P12 ($n=5$ at each time point) compared with controls ($n=4$ at each time point). (**d**) Early increase in plasma creatinine levels in mutants at P4 ($n=5$) as compared with controls ($n=4$). * Denotes $P<0.05$ by *t*-test.

Ultrastructural characterization of glomerular lesions

Electron microscopic studies of controls (Figure 6a and d) and littermate mutant mice (Figure 6b, c, and e) at P10 revealed extensive changes affecting not only the podocytes but also the mesangial and endothelial compartments. Villous transformation of podocytes is evident along with extensive vacuolization (Figure 6b) and foot process effacement (Figure 6c). In rare areas where foot processes were preserved, these were noted to be closely apposed without any visible slit diaphragm (Figure 6e), in contrast with control mice (Figure 6d). Widening of the sub-endothelial space due to endothelial cell swelling was observed, leading to uneven glomerular capillary wall thickening (Figure 6c). Although endothelial fenestrae were focally preserved, they were more frequently replaced by a continuous cytoplasmic layer lining the periphery of the capillary loops. Irregular edematous infiltration of the mesangial areas with disruption of the mesangial strands and focal detachment of the mesangial cells were present (Figure 6b and c).

Gene expression profile in mutant podocin mice

Finally, we used real-time PCR to investigate the effects of mutant R140Q podocin on the gene expression profile in the whole kidney at P4 and P12 (Table 1). We observed an insignificant decrease in *Nphs1* levels in *Nphs2*$^{R140Q/R140Q}$ mice, whereas *Cd2ap* mRNA levels were upregulated. No clearly significant changes were noted in either *Trpc6* or *Plce1* expression levels. Expression levels of transcription factors implicated in glomerular function were assessed and revealed transient, early upregulation of *Wt1* and a late downregulation of *Lmx1b*. On the other hand, sustained elevations in the transcriptional levels of the *Tcf21* (encoding Pod1 transcription factor), *Mafb* (encoding Kreisler transcription factor) and the *Zhx1-3* genes were measured in *Nphs2*$^{R140Q/R140Q}$ mice (Table 1). Given the prominent mesangial lesions, including sclerosis, in these mice, the levels of expression of the *Vegfa*, *Serpine1* (encoding plasminogen activator inhibitor-1), and *Tgfb1* genes were quantified. In mutant mice, although *Vegfa* levels were initially increased, they subsequently decreased by P12. On the contrary, sustained upregulation of *Serpine1* and *Tgfβ1* expression levels were observed in *Nphs2*$^{R140Q/R140Q}$ mice.

The gene expression profile was compared with that of constitutive podocin-knockout, mice. Despite similarities in renal phenotypes, the levels of *Nphs1*, *Trpc6*, and *Plce1* genes were markedly downregulated in podocin-null mice at P12 (Table 1). Additionally, we found no increases in *Mafb*, *Zhx2*, or *Tgfb1* levels, which were instead unchanged or decreased.

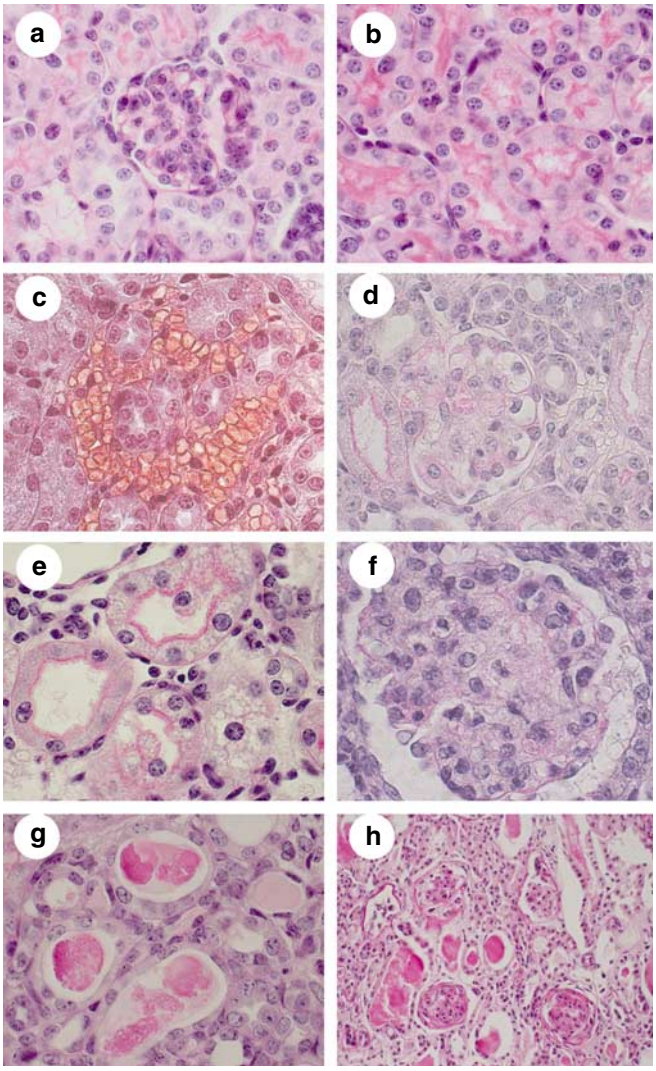

Figure 5 | Evolution of renal histological lesions in mutant mice. (**a**, **b**) Normal glomeruli and tubules seen in periodic acid–Schiff-stained sections from *Nphs2*$^{+/+}$ mice at P12. Wild-type mice at P4 are identical and are not shown. (**c**) Interstitial hemorrhages are seen in the cortical and juxtamedullary regions of mutant mice at P4. Section stained with Masson's trichrome-light green. (**d**) Periodic acid–Schiff-stained section from a mutant mouse at P4 demonstrating mesangial expansion, mesangiolysis, and capillary dilatation. (**e**) Focal tubular dilation and vacuolization are present in mutant mice at P4. (**f**) Progression of mesangiolysis and obstruction of glomerular capillary loops seen in a periodic acid–Schiff-stained section of a mutant mouse at P12. (**g**) Tubular dilation and protein casts are present in mutant mice at P12. (**h**) Diffuse and global glomerulosclerosis and severe tubulointerstitial lesions in a mutant mouse at P32. Original magnification $\times$1000 (**a**–**g**); $\times$200 (**h**).

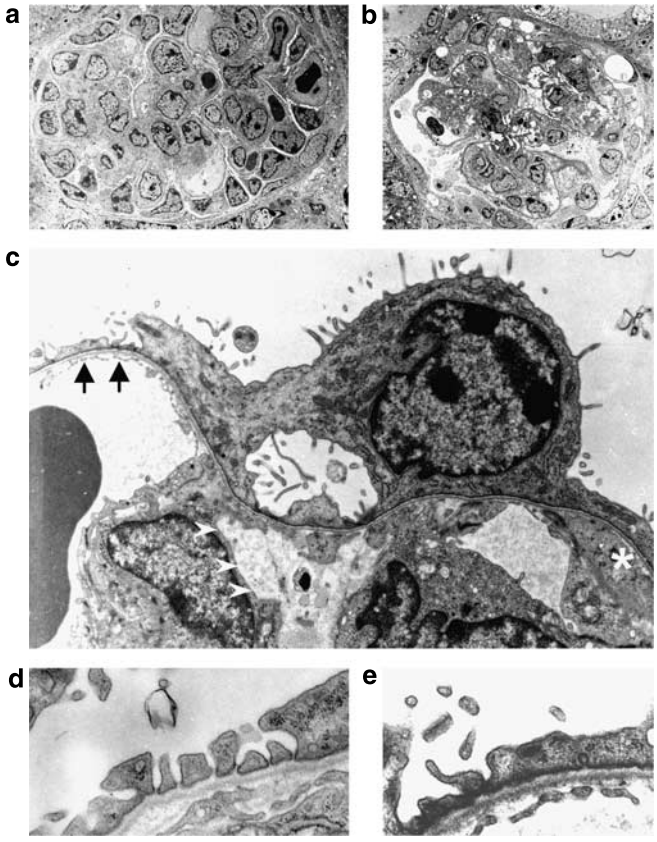

Figure 6 | Ultrastructural abnormalities in mutant podocin mice. Electron microscopy performed on P10 kidneys from *Nphs2*$^{+/+}$ (**a**, **d**) and *Nphs2*$^{R140Q/R140Q}$ (**b**, **c**, and **e**) mice. (**b**) Extensive changes seen in the glomeruli of *Nphs2*$^{R140Q/R140Q}$ mice, including, podocyte vacuolization, disorganization of the mesangial stalks with presence of edematous areas, and reduced patency of capillary lumina. Original magnification $\times$1100. (**c**) Podocytes in *Nphs2*$^{R140Q/R140Q}$ mice demonstrate foot process effacement and microvillous transformation. Black arrows indicate an area where endothelial fenestrations are preserved. Endothelial cell swelling is present (designated by *). White arrowheads show areas of mesangial edema. Original magnification $\times$6000. (**d**) Podocyte foot processes in wild-type mice are regularly spaced with slit diaphragm in between (original magnification $\times$7900), whereas (**e**) the foot processes are partially effaced in *Nphs2*$^{R140Q/R140Q}$ and have no slit diaphragms (original magnification $\times$5300).

Moreover, the *Zhx1* gene was downregulated at P12. On the contrary, both *Vegfa* and *Serpine1* were similarly perturbed with loss of podocin.

DISCUSSION

Mutations in the *NPHS2* gene account for 43% of familial autosomal recessive and 10.5% of sporadic cases of steroid-resistant nephrotic syndrome.[2] Among these, missense variants account for a significant proportion of pathogenic mutations. We have previously found that the age of onset of nephrotic syndrome in patients with *NPHS2* missense mutations correlates with the ability of podocin mutants, during *in vitro* studies, to traffic correctly in the cell.[6] Podocin mutants able to reach the plasma membrane are associated with later onset than mutants retained in the endoplasmic reticulum.[6] The p.R138Q mutant represents the most common mutation found in our cohort of patients, and has been shown to be retained in the endoplasmic reticulum.[6,10] Furthermore, Huber *et al.*[9] have shown that this results in failure of nephrin to reach specialized lipid raft microdomains, thereby abrogating the ability of podocin to enhance nephrin-mediated activator protein-1 activity. Immunohistochemical studies have, indeed, confirmed an alteration in nephrin distribution in glomeruli obtained from

Table 1 | Gene expression profile in *Nphs2*$^{R140Q/R140Q}$ mice compared with *Nphs2*$^{-/-}$ mice

		Nphs2$^{R140Q/R140Q}$		*Nphs2*$^{-/-}$	
		Expression levels (vs control)		Expression levels (vs control)	
Gene	Protein	P4	P12	P5	P12
Nphs1	Nephrin	0.80 ± 0.19	0.87 ± 0.20	1.94 ± 0.84	0.58 ± 0.20*
Cd2ap	CD2-associated protein	1.83 ± 0.43*	1.52 ± 0.19	1.38 ± 0.17	1.05 ± 0.15
Trpc6	Transient receptor potential channel 6	Undetectable	0.92 ± 0.33	1.06 ± 0.53	0.48 ± 0.11§
Plce1	Phospholipase Cε-1	1.31 ± 0.24	0.91 ± 0.20	1.96 ± 0.81	0.45 ± 0.21*
Wt1	Wilms' tumor homolog	1.43 ± 0.43	1.01 ± 0.38	1.09 ± 0.21	0.79 ± 0.20
Lmx1b	Lmx1b transcription factor	1.09 ± 0.38	0.64 ± 0.37	0.93 ± 0.22	0.72 ± 0.28
Tcf21	Transcription factor 21 (Pod1)	1.37 ± 0.36	1.47 ± 0.30	0.78 ± 0.21	0.81 ± 0.27
Mafb	v-maf oncogene family protein B (Kreisler transcription factor)	1.84 ± 0.43	2.29 ± 0.90*	1.05 ± 0.33	0.83 ± 0.29
Zhx1	Zinc fingers and homeoboxes 1	1.80 ± 0.32	1.56 ± 0.50	0.80 ± 0.13	0.67 ± 0.13*
Zhx2	Zinc fingers and homeoboxes 2	1.50 ± 0.40	1.86 ± 0.70*	1.14 ± 0.24	0.77 ± 0.31
Zhx3	Zinc fingers and homeoboxes 3	1.82 ± 0.49	1.29 ± 0.36	1.01 ± 0.40	0.99 ± 0.46
Vegfa	Vascular endothelial growth factor-A	1.50 ± 0.25	0.59 ± 0.09	0.83 ± 0.17	0.59 ± 0.18§
Serpine1	Plasminogen activator inhibitor-1	5.43 ± 1.98*	7.98 ± 2.62*	4.26 ± 0.77*	4.28 ± 1.62§
Tgfb1	Transforming growth factor-β	1.44 ± 0.26	2.07 ± 0.60*	1.27 ± 0.28	0.90 ± 0.14

Real-time PCR from kidneys of mice at P4 and P12 showed dysregulation of multiple genes in mutant *Nphs2*$^{R140Q/R140Q}$ mice (n=6, n=5 at P4 and P12, respectively) compared with wild-type mice (n=4 at each time point). Expression profiling was similarly performed in *Nphs2*-null mice at P5 and P12 (n=5 at each time point) and compared with controls (n=4 at each time point). Values are mean ± s.d. and reflect fold change vs controls using *18S rRNA* as endogenous control, and calculated using the $2^{-\Delta\Delta}C_t$ method. *$P<0.05$; §$P<0.01$.

renal biopsies of *NPHS2* patients.[14] Interestingly, a recent study identified carriers of the p.R138Q mutation to be at 4.9-times greater risk of developing FSGS, suggesting that mislocalization of podocin may have pathological consequences even in the heterozygous state.[15]

We believed that an *in vivo* system in which mutant podocin protein is expressed in mice would provide insight into the fate of abnormal proteins arising from common missense mutations. Furthermore, recent studies have shown that mutant proteins retained in the endoplasmic reticulum may be aided by pharmacological interventions to reach the plasma membrane,[16,17] thereby increasing the value of a murine model. To this end, we generated a novel mouse model in which the R140Q podocin mutant, the equivalent of the p.R138Q mutation in humans, is expressed in the kidney.

Successful targeting of the murine *Nphs2* allele by homologous recombination led to the expression of the R140Q variant, confirmed at the mRNA and protein levels. Interestingly, we found that although mRNA levels of podocin are upregulated, the corresponding protein levels are significantly lower. Immunohistochemical studies confirmed that mutant podocin is expressed in the cell, but is mislocalized to cytoplasmic compartments. It is probable that the R140Q variant is misfolded and consequently targeted for degradation in proteasome.[18] Additionally, our data demonstrate that this triggers mistargeting of only part of the nephrin pool in the cell, but suggest that nephrin trafficking may also occur via podocin-independent mechanisms.

In effect, *Nphs2*$^{R140Q/R140Q}$ mice recapitulate the renal phenotypes seen in mice with constitutive loss of podocin,[12] suggesting that the R140Q mutation is a loss-of-function allele. Similar to patients bearing the p.R138Q mutation, these mice develop albuminuria early, associated with widespread foot process effacement and progress to terminal renal failure within the first month of life. However, as opposed to *NPHS2* patients in whom renal lesions range from minimal change disease to focal and segmental glomerulosclerosis,[1] these mice develop renal lesions of mesangiolysis progressing to diffuse mesangial sclerosis, and ultrastructural evidence of endothelial lesions. Interestingly, podocyte-specific inactivation of podocin in the mature kidney leads to renal histological lesions of FSGS, reminiscent of the human disease (Esquivel EL, Mollet G, Lavin TA *et al.* (Abstract) *J Am Soc Nephrol* 2006; **17**: 24A). These findings suggest that during the process of glomerulogenesis, which continues during the first two weeks of life in mice, inactivation of podocin or podocyte injury or mediators present in the nephrotic milieu may lead to significant disturbance of podocyte–endothelial cell–mesangial cross talk. Indeed, Eremina *et al.*[19] have shown that mesangiolysis occurs when crucial signals from the podocyte, mediated by vascular endothelial growth factor-A and likely acting through the endothelial cells, are disrupted during glomerulogenesis. Technical difficulties limited our ability to obtain a gene expression profile limited to the renal glomerulus. However, results from profiling of whole kidneys revealed that the vascular endothelial growth factor pathway is perturbed, and may account for the development of mesangial and endothelial lesions.

Taking these limitations into consideration, quantitative PCR revealed a modest, early upregulation of *Cd2ap* transcription, as seen in podocin-null mice[12] and during *in vitro* studies.[20] However, levels of other podocyte-expressed genes are not robustly altered, but we cannot exclude that additional perturbation occurs at the post-transcriptional level or in pathways involved in protein degradation. CD2AP binds to podocin and may provide a crucial link to the actin cytoskeleton,[7] the remodelling of which is involved in podocyte foot process effacement. It has previously been

shown that CD2AP and podocin are targets of the LMX1B transcription factor.[21] Our data, however, demonstrate a trend toward subsequent downregulation of *Lmx1b* in the course of renal disease evolution. One recent study has shown that overexpression of the ZHX2 transcription factor in a cell culture model leads to a downregulation of the *LMX1B* gene.[22] Curiously, the levels of the ZHX transcription factors decreased during the evolution of proteinuric renal disease in a rat model of nephrotic syndrome.[22] In contrast, we found that *Zhx2* transcriptional levels, exclusively expressed in podocytes in the kidney,[22] were upregulated in our model. Moreover, upregulation of the Kreisler transcription factor was measured, but its downstream targets in the podocyte are unclear. Additional work will be necessary to better understand the complex interactions among these different genes in the course of renal disease evolution.

Additionally, our data provide further evidence of involvement of the plasminogen activator inhibitor-1 and transforming growth factor-β pathways in glomerular disease. Prior studies have demonstrated an involvement of these growth factors in the pathogenesis of mesangiolysis[23] and diffuse mesangial sclerosis.[24] Moreover, these are known mediators of the pathophysiological mechanisms involved in chronic kidney disease progression.[25,26] We likewise demonstrated genetic modification of the survival of these mutant mice, with 129-enriched mutant mice surviving longer. It will be of interest in the future to examine whether differential regulation of the plasminogen activator-inhibitor-1 and transforming growth factor-β pathways may play a role in phenotypic modification by genetic factors.

Finally, we demonstrated that despite similarities in the renal phenotypes of R140Q mutant and *Nphs2*-null mice, there are distinct differences in the expression profiles of select genes in the glomerulus, particularly those involved in structural integrity and transcriptional regulation. On the other hand, genes involved in progression were similarly perturbed. These discrepancies may reflect discrete pathways perturbed in the presence of a mutant, misfolded protein necessitating engagement of degradation pathways. Alternatively, they may arise from differences in genetic background, since the *Nphs2*-null mice examined were 129 congenics, whereas the mutant mice were only 129-enriched.

MATERIALS AND METHODS

Generation of *Nphs2*$^{R140Q/R140Q}$ mice

A 6.6-fragment containing exons 3 and 4 was obtained after *Hin*dIII digestion of genomic DNA and the 3′ *Hin*dIII site was mutated to a *Not*I site and inserted into the pBluescriptIIKS vector (Stratagene, La Jolla, CA, USA). Site-directed mutagenesis (Quick-Change kit; Stratagene) was used to introduce the c.505G>A, c.506A>G mutations, which created a *Pvu*II site in exon 3. A floxed hygromycin cassette (phosphoglycerate kinase–hygromycin) was inserted in reverse orientation into intron 3 via an *Sma*I site generated by site-directed mutagenesis.

The targeting vector was electroporated into 129S2/SvPAS embryonic stem cells and selected in hygromycin-containing medium. Hygromycin-resistant embryonic stem cell clones were screened by Southern blot hybridization using internal and external probes (Figure S1). Two clones were expanded and injected into C57BL/6 blastocysts. Mice with greater than 80% chimerism were mated to obtain germline transmission. Tail biopsies were performed and genotyping was carried out by PCR using primers (5′-CCACTTGTGTAGCGCCAA-3′ and 5′-TTGGGAGAAGAGGCA CAG-3′) flanking the hygromycin cassette and a protocol consisting of denaturation at 94 °C for 5 min followed by 35 cycles of denaturation at 94 °C for 1 min, annealing at 55 °C for 1 min and extension at 72 °C for 1 min, and a final extension step at 72 °C for 7 min. These mice were mated with Meu-Cre 40 mice constitutively expressing Cre recombinase,[13] excising the floxed hygromycin cassette. Heterozygous *Nphs2*$^{R140Q/+}$ mice were mated with wild-type mice to select out the Cre recombinase gene and intercrossed to produce homozygous *Nphs2*$^{R140Q/R140Q}$ mice on a mixed B6-129 genetic background. The *Nphs2*^{R140Q} allele was backcrossed onto the 129S2/SvPas genetic background for three generations, enriching 129 alleles to about 75% content.

Mice were maintained in a specific pathogen-free environment and experiments were conducted in compliance with ethical standards established by the French government and by the ethical committees of Inserm, Paris and Hôpital Necker.

Genotyping

Tail genomic DNA was extracted using the Nucleospin Tissue kit (Macherey-Nagel, Hoerdt, France) and PCR was performed using primers flanking exon 3 (5′-CGAGTGGCTTCTTGTCCT-3′ and 5′-GAGACGGAGATCAACCTTGT-3′). The PCR protocol consisted of an initial denaturation step at 94 °C for 5 min, followed by 35 cycles of denaturation at 94 °C for 1 min, annealing at 55 °C for 1 min, and extension at 72 °C for 1 min, and a final extension step at 72 °C for 7 min. PCR products were digested using *Pvu*II enzyme (NE Biolabs, Ipswich, MA, USA) and separated on a 2% agarose gel, revealing a 184-bp wild-type allele, and 80 and 104-bp bands (not resolved) in heterozygous and homozygous mutant mice (Figure S2).

RNA extraction and real-time PCR

Total RNA was extracted from the kidneys of control ($n=5$) and mutant ($n=6$ at P4 and $n=5$ at P12) mice killed at P4 and P12, using TRIzol reagent (Invitrogen, Carlsbad, CA, USA). Similarly, controls and *Nphs2*-null mice were killed at P5 and P12 ($n=4$ and $n=5$ of each genotype and time point) and kidney RNA was extracted. Northern blot hybridization was performed using ^{32}P-labelled cDNA consisting of exons 1 to 8 of the mouse *Nphs2* gene. Reverse transcription with random primers was performed on 500 ng of total RNA using SuperscriptII reverse transcriptase (Invitrogen). Real-time PCR was performed on a TaqMan ABI Prism 7700 Sequence Detection System (Applied Biosystems, Foster City, CA, USA) using Absolute QPCR mix (Thermo Fisher Scientific, Waltham, MA, USA) and pre-designed Assays-on-Demand primers and probes (Applied Biosystems). Assays were performed in duplicates and water controls were run as negatives. Relative quantification of gene expression was performed using the $2^{-\Delta\Delta}C_t$ method and *18S rRNA* as endogenous controls.[27]

Western blot

Kidneys from control and mutant mice at P1 (data not shown) and P12 were removed and lysed in buffer containing 0.5% CHAPS, 20 mM Tris, pH 7.5, 500 mM NaCl, and protease inhibitors (Complete Mini, Roche, Basel, Switzerland). A 20-μg weight of

protein lysates was separated on a 12% sodium dodecyl sulfate-polyacrylamide gel electrophoresis denaturing gel and transferred to nitrocellulose Transfer Membrane (Schleicher & Schuell, Dassel, Germany). The membrane was blocked with 5% low-fat milk, 2% bovine serum albumin in Tween–Tris-buffered saline (TTBS) and incubated overnight at 4 °C with rabbit polyclonal anti-podocin antibody (Sigma, St Louis, MO, USA) at 1:2000 dilution. After several washes with 1 × TTBS, membranes were incubated for 1 h with anti-rabbit IgG horseradish peroxidase-linked antibody (Cell Signaling, Danvers, MA, USA) diluted 1:2000 in blocking buffer. Signals were revealed using the ECL system (GE Healthcare, Buckinghamshire, England). Blots were reprobed with anti-CBP80 antibodies (kindly provided by Elisa Izaurralde, EMBL Heidelberg) diluted 1:1000, after stripping with Restore Western Blot Stripping buffer (Pierce, Rockford, IL, USA).

Urine and blood analyses

Blood was collected in heparinized tubes when mice were killed. Plasma was obtained after centrifugation at 5000 *g* for 10 min. Plasma chemistries were performed using an Olympus AU-400 multiparametric analyzer (Hôpital Bichat, Paris, France). Urine was collected by bladder puncture and 2 µl were analyzed on a 10% sodium dodecyl sulfate-polyacrylamide gel electrophoresis gel, followed by Coomassie blue staining.

Histological analysis

Kidneys were fixed in alcoholic Bouin for 2 h, dehydrated, and embedded in paraffin. Four-micrometer-thick sections were stained with Masson's Trichrome-light green or periodic acid–Schiff and examined under a Leitz Orthoplan microscope (Leica Microsystems GmbH, Wetzlar, Germany). For electron microscopy, tissue samples were processed as previously described,[28] and samples from littermate controls were systematically examined under identical conditions.

Immunohistochemical studies

Immunofluorescence staining was performed as described.[12] Acet-one-fixed sections (6–7 µm) were simultaneously incubated with rabbit anti-podocin[28] (diluted 1:500) or guinea pig anti-nephrin (diluted 1:50; Progen, Heidelberg, Germany) and rat anti-nidogen (diluted 1:100; Millipore, Billerica, MA, USA) antibodies. After rinsing, slides were incubated with appropriate secondary Alexa Fluor-conjugated antibodies (Invitrogen). Nuclei were labelled using 0.75 µg ml^{-1} propidium iodide (Sigma). Slides were examined using a Zeiss confocal microscope (Carl Zeiss, Jena, Germany).

Statistical analyses

Values are reported as mean ± s.e.m. Statistical comparisons were performed using either Student's *t*-test or Mann–Whitney test as appropriate. $P < 0.05$ was considered significant.

DISCLOSURE

The authors report no conflict of interest.

ACKNOWLEDGMENTS

We thank Marco Giovannini and Séverine Roselli for providing the targeting vector, Martin Holtzenberg for providing the Meu-Cre 40 mice, and Elisa Izaurralde for providing the anti-CBP80 antibodies. We are grateful to Bärbel Phillipin and Hiltraut Hosser for excellent technical assistance and to Meriem Garfa for assistance with confocal microscopy. This study was supported by the Ministère de l'Enseignement Supérieur et de la Recherche and Fondation pour la Recherche Médicale (PhD grants for AP), the PROCOPE program of EGIDE/DAAD (project number 07521ZJ to SW), and the Deutsche Forschungsgemeinschaft (WE 2724/2-1 and WE 2724/2-2 to SW). Additional funding was obtained from the EuReGene Project, an integrated project (5085) in Framework Program 6 of the European Commission (to CA), and the Association pour l'Utilisation du Rein Artificiel (to CA).

SUPPLEMENTARY MATERIAL

Figure S1. Identification of correctly targeted ES cells by Southern blot hybridization.
Figure S2. Genotyping of mutant mice.

REFERENCES

1. Boute N, Gribouval O, Roselli S *et al. NPHS2* encoding the glomerular protein podocin is mutated in autosomal recessive steroid-resistant nephrotic syndrome. *Nat Genet* 2000; **24**: 349–354.
2. Weber S, Gribouval O, Esquivel EL *et al. NPHS2* mutation analysis shows genetic heterogeneity of steroid-resistant nephrotic syndrome and low post-transplant recurrence. *Kidney Int* 2004; **66**: 571–579.
3. Karle SM, Uetz B, Ronner V *et al.* Novel mutations in *NPHS2* detected in both familial and sporadic steroid-resistant nephrotic syndrome. *J Am Soc Nephrol* 2002; **13**: 388–393.
4. Hinkes BG, Mucha B, Vlangos CN *et al.* Nephrotic syndrome in the first year of life: two thirds of cases are caused by mutations in 4 genes (*NPHS1*, *NPHS2*, *WT1*, and *LAMB2*). *Pediatrics* 2007; **119**: e907–e919.
5. Tsukaguchi H, Sudhakar A, Le TC *et al. NPHS2* mutations in late-onset focal segmental glomerulosclerosis: R229Q is a common disease-associated allele. *J Clin Invest* 2002; **110**: 1659–1666.
6. Roselli S, Moutkine I, Gribouval O *et al.* Plasma membrane targeting of podocin through the classical exocytic pathway: effect of *NPHS2* mutations. *Traffic* 2004; **5**: 37–44.
7. Schwarz K, Simons M, Reiser J *et al.* Podocin, a raft-associated component of the glomerular slit diaphragm, interacts with CD2AP and nephrin. *J Clin Invest* 2001; **108**: 1621–1629.
8. Benzing T. Signaling at the slit diaphragm. *J Am Soc Nephrol* 2004; **15**: 1382–1391.
9. Huber TB, Simons M, Hartleben B *et al.* Molecular basis of the functional podocin-nephrin complex: mutations in the *NPHS2* gene disrupt nephrin targeting to lipid raft microdomains. *Hum Mol Genet* 2003; **12**: 3397–3405.
10. Nishibori Y, Liu L, Hosoyamada M *et al.* Disease-causing missense mutations in *NPHS2* gene alter normal nephrin trafficking to the plasma membrane. *Kidney Int* 2004; **66**: 1755–1765.
11. Huber TB, Schermer B, Muller RU *et al.* Podocin and MEC-2 bind cholesterol to regulate the activity of associated ion channels. *Proc Natl Acad Sci USA* 2006; **103**: 17079–17086.
12. Roselli S, Heidet L, Sich M *et al.* Early glomerular filtration defect and severe renal disease in podocin-deficient mice. *Mol Cell Biol* 2004; **24**: 550–560.
13. Leneuve P, Colnot S, Hamard G *et al.* Cre-mediated germline mosaicism: a new transgenic mouse for the selective removal of residual markers from tri-lox conditional alleles. *Nucleic Acids Res* 2003; **31**: e21.
14. Zhang SY, Marlier A, Gribouval O *et al. In vivo* expression of podocyte slit diaphragm-associated proteins in nephrotic patients with NPHS2 mutation. *Kidney Int* 2004; **66**: 945–954.
15. McKenzie LM, Hendrickson SL, Briggs WA *et al. NPHS2* variation in sporadic focal segmental glomerulosclerosis. *J Am Soc Nephrol* 2007; **18**: 2987–2995.
16. Egan ME, Pearson M, Weiner SA *et al.* Curcumin, a major constituent of turmeric, corrects cystic fibrosis defects. *Science* 2004; **304**: 600–602.
17. Liu XL, Done SC, Yan K *et al.* Defective trafficking of nephrin missense mutants rescued by a chemical chaperone. *J Am Soc Nephrol* 2004; **15**: 1731–1738.
18. Ellgaard L, Helenius A. Quality control in the endoplasmic reticulum. *Nat Rev Mol Cell Biol* 2003; **4**: 181–191.
19. Eremina V, Cui S, Gerber H *et al.* Vascular endothelial growth factor a signaling in the podocyte-endothelial compartment is required for mesangial cell migration and survival. *J Am Soc Nephrol* 2006; **17**: 724–735.
20. Fan Q, Xing Y, Ding J *et al.* The relationship among nephrin, podocin, CD2AP, and alpha-actinin might not be a true 'interaction' in podocyte. *Kidney Int* 2006; **69**: 1207–1215.

21. Rohr C, Prestel J, Heidet L *et al.* The LIM-homeodomain transcription factor Lmx1b plays a crucial role in podocytes. *J Clin Invest* 2002; **109**: 1073–1082.
22. Liu G, Clement LC, Kanwar YS *et al.* ZHX proteins regulate podocyte gene expression during the development of nephrotic syndrome. *J Biol Chem* 2006; **281**: 39681–39692.
23. Barnes JL, Mitchell RJ, Torres ES. Expression of plasminogen activator-inhibitor-1 (PAI-1) during cellular remodeling in proliferative glomerulonephritis in the rat. *J Histochem Cytochem* 1995; **43**: 895–905.
24. Yang Y, Zhang SY, Sich M *et al.* Glomerular extracellular matrix and growth factors in diffuse mesangial sclerosis. *Pediatr Nephrol* 2001; **16**: 429–438.
25. Eddy AA, Fogo AB. Plasminogen activator inhibitor-1 in chronic kidney disease: evidence and mechanisms of action. *J Am Soc Nephrol* 2006; **17**: 2999–3012.
26. Schiffer M, von Gersdorff G, Bitzer M *et al.* Smad proteins and transforming growth factor-beta signaling. *Kidney Int Suppl* 2000; **77**: S45–S52.
27. Livak KJ, Schmittgen TD. Analysis of relative gene expression data using real-time quantitative PCR and the 2(−delta delta C(T)) method. *Methods* 2001; **25**: 402–408.
28. Roselli S, Gribouval O, Boute N *et al.* Podocin localizes in the kidney to the slit diaphragm area. *Am J Pathol* 2002; **160**: 131–139.